An analysis of pore pressure measurement in gassy soils

Xu, Man; Jommi, Cristina; Muraro, Stefano

Important note
To cite this publication, please use the final published version (if applicable).
Please check the document version above.

An analysis of pore pressure measurement in gassy soils

Man Xu[1,*], *Cristina* Jommi[1,2] , and *Stefano* Muraro[1]

[1] Delft University of Technology, Department of Geosciences and Engineering, Stevinweg 1 2628CN Delft, The Netherlands

[2] Politecnico di Milano, Dipartimento di Ingegneria Civile e Ambientale, Piazza Leonardo da Vinci 32 20133 Milano, Italy

Abstract. The presence of entrapped gas, formed by the degradation of organic matter, complicates the pore pressure measurement in gassy soils. To address this challenge, fully coupled hydro-mechanical finite element simulations are presented to analyse the pore pressure response observed from triaxial tests of gassy peat samples. The experiments incorporated novel local pore pressure transducers, able to track distinct pore pressure measurements at separate locations. By replicating the experimental tests, the numerical simulations assessed the effects of non-uniform gas concentration and soil-porous disk interactions to refine gassy soil testing procedures and improve data interpretation.

1 Introduction

In-situ observations suggest the presence of entrapped gas bubbles within organic soft soil layers. The decomposition of organic matter saturates the pore fluid with gas species such as CH_4, H_2S, and CO_2. When their concentration exceeds equilibrium solubility, dissolved gases can exsolve due to anthropogenic activities, such as excavation and dewatering, as well as environmental factors like temperature increase and atmospheric pressure fluctuation. Evidence from closed piezometers pore pressure responses [1], seasonal surface elevation oscillations [2], and CPT camera soundings [3] confirm the presence of gas within peat layers. The occurrence of free gas in soils poses a potential risk to the serviceability and stability of earth infrastructure, prompting recent laboratory investigations to assess its effects on organic soils [4, 5].

As of today, the majority of the laboratory tests on gassy samples have been performed with standard triaxial apparatuses equipped with a single pore pressure transducer below the porous disk, without assessing the reliability of the transducer response under gassy conditions. Additionally, the homogeneity of dissolved gas within the sample, particularly when flushing is used to replace the in-situ pore fluid with gas-charged artificial fluid [4, 6], has not been assessed. Numerical modelling [7] serves as a valuable tool to gain insight into the pore pressure responses in gassy soils and to support the definition of laboratory testing protocols.

This research bridges the gap between experimental observations and numerical simulations, aiming to analyse pore pressure measurement and the underlying mechanisms during the gas exsolution process.

2 Experimental observations

Natural peat samples extracted from Leendert de Boerspolder dyke in the Netherlands were tested in gassy conditions. Table 1 presents the index properties of samples.

Gassy tests were performed on peat samples using a quasi-dynamic triaxial apparatus equipped with lateral local pore pressure transducers [8]. The tested cylindrical samples measure 50 mm in diameter and 110 mm in height. The intended insertion depth of the pore pressure transducer probe within the sample is 5 mm.

Table 1. Index properties of tested samples.

Label	e_0 (-)	w_0 (-)	G_s (-)	$S_{r,0}$ (-)	γ (kN/m³)
Test 1	10.83	6.72	1.498	0.929	9.59
Test 2	10.80	6.96	1.498	0.965	9.91

The approach proposed by Sultan *et al*. (2012) [6] and Jommi *et al*. (2019) [4] was adopted in the experimental tests. After isotropic consolidation up to 20 kPa, the sample pore fluid was replaced with undersaturated CO_2-charged water by applying a pressure difference between the top and bottom drainage lines with two back pressure-volume controllers. The pore fluid was circulated from bottom to top, and the circulated volume was controlled at 3 times the volume of the sample. Dissolved gas was subsequently exsolved within the sample through isotropic undrained unloading at a rate of 100 kPa/h. The room conditions were maintained at a controlled temperature of 14°C and a relative humidity of 68% during both the preparation of the carbonated water and experiments.

---

[*] Corresponding author: m.xu-3@tudelft.nl

Fig. 1 and 2 present the response during the isotropic unloading stage in terms of mean operative stress and degree of saturation. The mean operative stress was calculated as the difference between radial stress and the pore pressure measured either from the lateral mid-plane transducer (MP) or standard pore water pressure transducers (PWP) beneath the porous disk. The degree of saturation was determined based on the calibrated relationship between cell pressure and cell volume, accounting for piston displacement. Test 1 shows a saturation of 97% and Test 2 of 89%, both within the typical range of degree of saturation representative of gassy soils, S_r >85% [9].

Fig. 1 illustrates the measurement discrepancies between the local transducers MP1 and MP2 during the desaturation process. The MP1 transducer, positioned at the mid-height of the sample, shows a smaller reduction in operative stress compared to MP2 and the pore water pressure (PWP) sensor at the sample bottom. This discrepancy may result from non-uniform vertical distribution of dissolved gas concentrations during flushing. In peat, preferential flow channels can develop due to variations in fibrous structure. Additionally, a divergence in measurements between MP2 and PWP emerges at a later stage in Test 1, despite their similar locations. A possible explanation is that MP2 is in direct contact with the sample, whereas PWP measures indirectly through a porous disk, suggesting that soil–porous disk interactions may influence the readings. This aspect will be further investigated through numerical simulations.
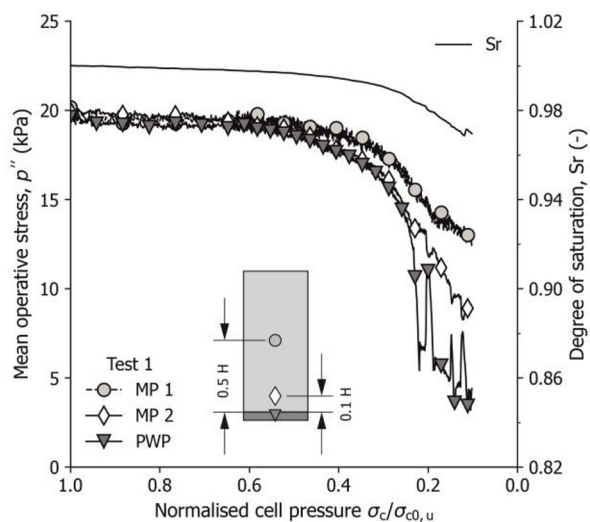
Fig. 1. Evolution of mean operative stress and degree of saturation during the isotropic undrained unloading of gassy peat with low gas nucleation (Test 1).

Fig. 2 illustrates differences in the measurements of MP and PWP transducers, which may result from a combined effect of the gas concentration gradient and soil-porous disk interaction. Additionally, from 2% desaturation onward, PWP measurements exhibit significant oscillations in both Test 1 and Test 2, raising questions about the reliability of pore pressure measurements in gassy conditions using a standard set up in the triaxial apparatus.
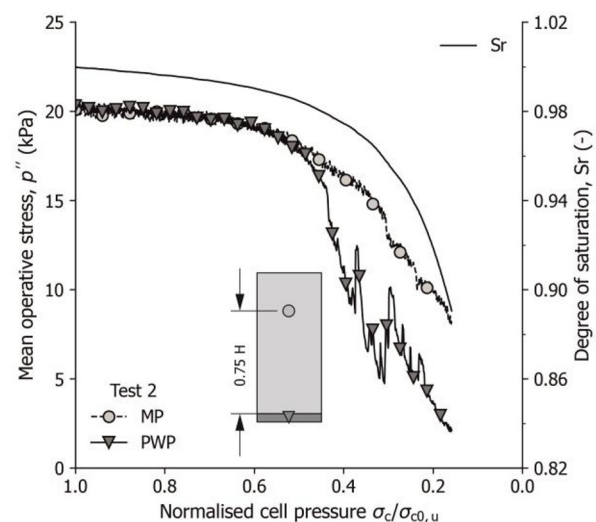
Fig. 2. Evolution of mean operative stress and degree of saturation during the isotropic undrained unloading of gassy peat with high gas nucleation (Test 2).

These experimental observations suggest that the effects of the gas concentration gradient and porous disk interaction require further investigation through numerical modelling. To explore this, Test 2 was reproduced using a finite element model to simulate pore pressure responses throughout the gas exsolution stage.

3 Finite element model

Three-phase fully coupled hydro-mechanical finite element simulations were conducted in a 2D axisymmetric framework using Code_Bright [10]. Fig. 3 illustrates the geometry of the problem. Simulations 1 and 2 were conducted without the presence of the porous disk underneath the sample while in Simulation 3 the porous disk (10 mm in inner radius and 3 mm in thickness) was modelled explicitly to assess the interaction of the two parts.
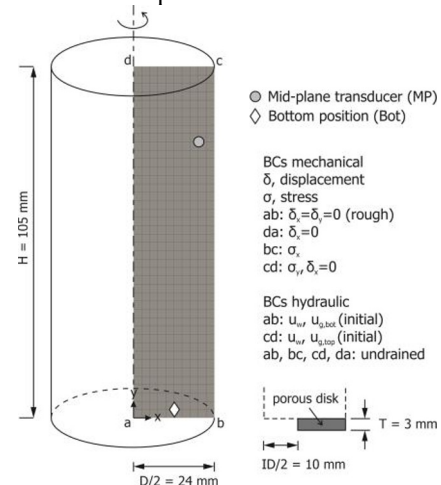
Fig. 3. Geometry of the problem in the FEM simulations.

The simulations were initialised with the stress conditions corresponding to the end of the CO_2-charged water flushing. An isotropic stress of 413 kPa and a uniform pore liquid pressure of 393 kPa were applied to replicate the experimental test. Two different dissolved

gas pressure conditions, detailed in Table 2, were considered. As a reference case, Simulation 1 assumed a uniform dissolved gas pressure of 190 kPa, estimated from the onset of gas exsolution in Test 2. In contrast, Simulations 2 and 3 incorporated a linear profile of dissolved gas pressure to account for potential non-uniform distributions, as suggested by the experimental results in Fig. 2. The bottom gas pressure was set at 190 kPa, while the top was fixed at 10 kPa. In the absence of direct experimental measurements of gas concentration gradients, the low gas pressure at the top represents a lower bound, allowing assessment of its impact on the observed pore pressure in laboratory tests.

It is important to note that during flushing, dissolved gas migrates with the pore fluid along preferential flow paths but also diffuses through the latex membrane. This diffusion further contributes to reducing the actual gas concentration. The unloading stage was simulated by isotropically reducing the radial stress at a rate of 100 kPa/h under liquid and gas undrained conditions.

Local pore pressure nodes are indicated in Fig. 3, representing mid-plane (MP) and bottom (Bot) measurements.

Table 2. Geometry and imposed distribution of gas pressure.

	Sim. 1	**Sim. 2**	**Sim. 3**
Geometry	Sample	Sample	Sample, porous disk
Imposed distribution of dissolved gas pressure	Uniform	Linear	Linear

The input parameters used in the numerical simulations are summarised in Table 3. For the peat sample, the relationship between gas-liquid equilibrium pressure and degree of saturation was derived from air-drying tests [11], while for the porous disk, it was determined using a mercury intrusion porosimetry test. The soil water retention curves (SWRC) for both the peat sample and the porous disk are presented in Fig. 4, where the experimental data are fitted using the Van Genuchten model [12].

The hydraulic conductivity of the tested peat, within the relevant void ratio range, was estimated based on the experimental results reported by Zhao and Jommi (2021) [13], while the relative hydraulic conductivity follows the experimental data from Trivellato (2014) [14]. The dissolved CO_2 concentration was defined using Henry's constant, H, evaluated at 14°C. To account for the initial presence of small occluded gas bubbles in the pore fluid at the start of unloading, due to the challenges of achieving full saturation, the compressibility of the liquid phase was set at 0.03 MPa⁻¹ [15]. The mechanical behaviour was modelled using the CASM framework [16] and extended to unsaturated conditions with Bishop stress. The CASM model parameters were estimated from a twin sample tested under saturated conditions. The porous disk was modelled as a linear elastic material with a Young's modulus of 100 MPa and a Poisson's ratio of 0.3.

Table 3. Constitutive laws and parameters used in finite element analysis for peat sample and porous disk.

Constitutive laws		**Parameters**
Soil water retention curve - Van Genuchten	$S_e = \dfrac{S_l - S_{rl}}{S_{ls} - S_{rl}} = \left[1 + \left(\dfrac{p_g - p_l}{P_0} \right)^{\frac{1}{1-\lambda}} \right]^{-\lambda}$	$S_{rl} = 0$ $S_{ls} = 1$ **Peat:** $P_0 = 25$ kPa $\lambda = 0.2$ **Porous disk:** $P_0 = 1.3$ kPa $\lambda = 0.7$
Intrinsic permeability - Darcy's Law	$q_\alpha = -\dfrac{k k_{r\alpha}}{\mu_\alpha}(\nabla p_\alpha - \rho_\alpha g)$	**Peat:** $k = 7\times10^{-8}$ m/s **Porous disk:** $k = 7\times10^{-5}$ m/s
Relative hydraulic conductivity	$k_{rl} = \sqrt{S_e}(1-(1-S_e^{1/\lambda})^\lambda)^2$	$\lambda = 0.25$
Relative gas conductivity	$k_{rg} = A S_{eg}^n$ $S_{eg} = \dfrac{S_g - S_{rg}}{S_{gs} - S_{rg}}$	$A = 1$ $n = 3$
Diffusive flux of air in the liquid phase - Fick's Law	$i_l^a = -(\tau \phi \rho_l S_l D_l^a I)\nabla \omega_l^a$ $D_l^a = D\exp(\dfrac{-Q}{R(273.15+T)})$	$\tau = 0.5$ $D = 4.2\times10^{-5}$ m²/s $Q = 24700$ J/mol
Dissolved gas concentration - Henry's Law	$\omega_l^a = \dfrac{p_a}{H}\dfrac{M_a}{M_w}$	$H = 111$ MPa⁻¹
Liquid phase density	$\rho_l = \rho_{l0}(1 - \beta(P_l - P_{l0}) + \alpha T + \gamma \omega_l^b)$	$\rho_{l0} = 1002.6$ kg m⁻³ $\beta = 0.03$ MPa⁻¹ $\alpha = -3.4\times10^{-4}$ C⁻¹ $\gamma = 0.6923$ $P_{l0} = 0.1013$ MPa
Mechanical – CASM with bishop stress	$f = (\dfrac{\sqrt{3}J}{M_\theta p'})^n + \dfrac{1}{\ln r}\ln\dfrac{p'}{p_0'}$ $\sigma_{ij}' = \sigma_{ij} - P_g\delta_{ij} + S_r s \delta_{ij}$ $dp_0' = \dfrac{p_0'(1+e_0)}{\lambda-\kappa}d\varepsilon_v^p$ $K = \dfrac{p'(1+e_0)}{\kappa}$ $G = \dfrac{3(1-2\nu)K}{2(1+\nu)}$	**Peat:** $\nu = 0.3$ $\kappa = 0.45$, $\lambda = 2.6$ $r = 2$, $n = 1.5$ $p_0' = 25$ kPa $M_\theta = 1.75$

S_e effective liquid degree of saturation, S_l liquid degree of saturation, S_{ls} maximum saturation, S_{rl} residual saturation, q_a liquid or gas phase flux, k_{rl} relative liquid conductivity, k_{rg} relative gas conductivity, S_{eg} effective gas degree of saturation, i_l^a dissolved gas diffusive flux, D_l^a dissolved molecular diffusion coefficient, ω_l^a mass fraction of dissolved gas, ϕ porosity, τ tortuosity coefficient, H Henry's constant, M_θ slope of critical state line, p_0' preconsolidation pressure, κ slope of unloading-reloading line, λ slope of normal consolidation line, ν Poisson's ratio.
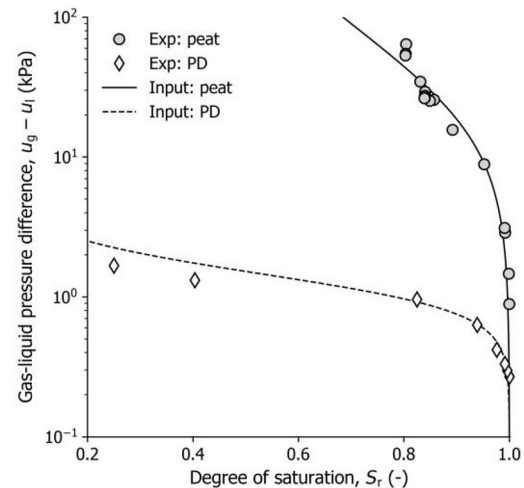

Fig. 4. Soil water retention curves for peat and porous disk.

4 Numerical results

The evolution of the mean operative stress during isotropic undrained unloading for Simulation 1 and 2 is presented in Fig. 5 and Fig. 6, respectively. The mean operative stress follows the concept of average skeleton stress from Jommi (2000) [16], calculated as

$$p'' = p - u_f$$
$$u_f = u_l + (1 - S_r)(u_g - u_l) \tag{1}$$

with u_f the average fluid pressure, S_r the local degree of saturation, u_l the liquid pressure, and u_g the gas pressure.
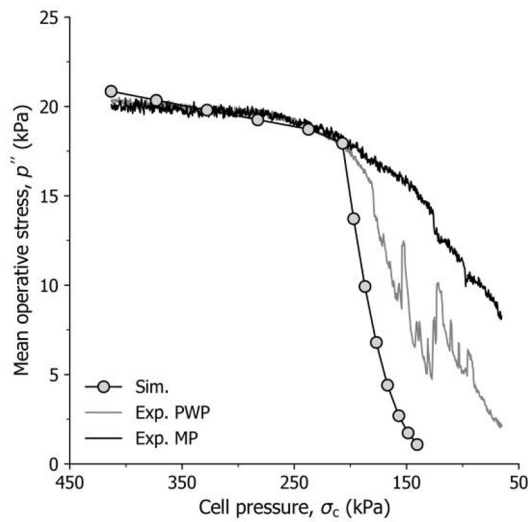

Fig. 5. Evolution of the mean operative stress during isotropic undrained unloading for Simulation 1 compared with laboratory Test 2.
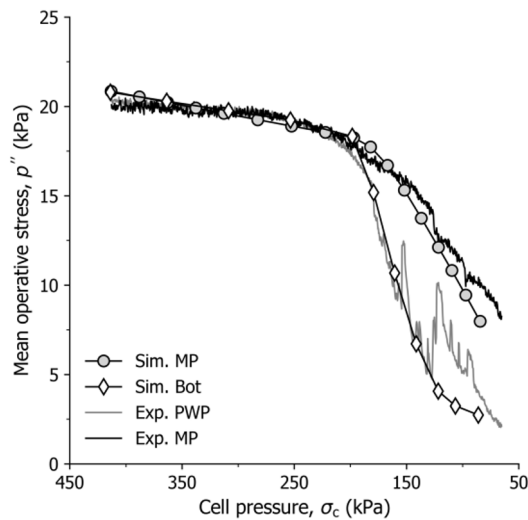

Fig. 6. Evolution of the mean operative stress during isotropic undrained unloading from MP and Bot measurements for Simulation 2 compared with laboratory Test 2.

In Simulation 1, the mean operative stress drops sharply after the onset of gas exsolution, failing to capture the transitional trend observed in the experiments. In contrast, Simulation 2, which incorporates a linear gas pressure distribution along the vertical axis, exhibits distinct mechanical responses at MP and Bot, effectively replicating the local pore pressure measurements. In both

simulations, the initial decrease in mean operative stress, up to a cell pressure of 200 kPa, is attributed to the non-negligible compressibility of the pore liquid, occurring before gas exsolution begins.
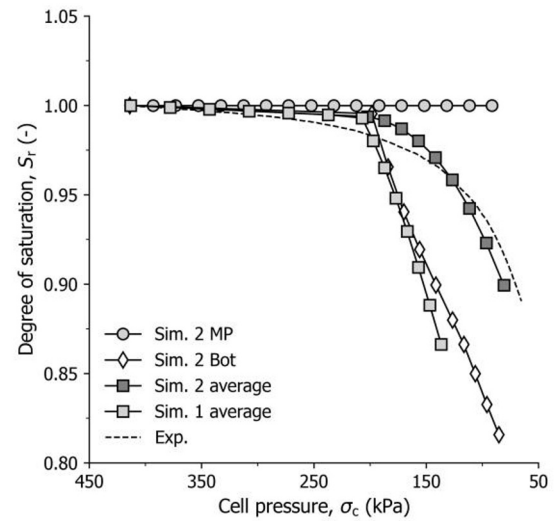

Fig. 7. Evolution of the degree of saturation for numerical simulations (local and average) and laboratory Test 2.

Fig. 7 reports the evolution of the degree of saturation obtained from the numerical simulations and the laboratory Test 2. For the numerical simulation, the results are presented in terms of local degree of saturation and average degree of saturation. The latter was calculated from the sample volume change by tracking the displacement of lateral nodes (boundary "bc" in Fig. 3). In both simulations, the initial decrease in average saturation is driven by the expansion of the liquid phase, which is influenced by its non-negligible compressibility. In Simulation 1, gas exsolution leads to a sharp drop in saturation once the gas-liquid equilibrium pressure is reached. In contrast, Simulation 2, which incorporates a non-uniform dissolved gas concentration, exhibits a more gradual desaturation process during undrained unloading, aligning more closely with experimental observations.

5 Discussion

5.1 Local pore pressure response

Interpreting the hydro-mechanical response of gassy soils is not straightforward as the sample experiences different desaturation stages during the tests, ranging from saturated conditions, small isolated gas bubbles and potentially locally interconnected gas clusters depending on the amount of the exsolved gas. This complicates the interpretation of pore pressure measurements in gassy soils which may not always reflect the liquid pressure due to potential interference of the gas phase in the proximity of the sensor. An insight is offered in Fig. 8 by analysing the results of Simulation 2 under two different assumptions: (i) the pore fluid pressure at the bottom of the sample is the liquid pressure, and (ii) it corresponds to the average fluid pressure, as defined in Equation (1). During the initial stage of undrained unloading, when the

amount of exsolved gas is minimal (S_r> 98%), both assumptions yield similar results. However, as gas exsolution progresses, the curves begin to diverge, with gas pressure exerting an increasing influence. The experimental data derived from pore pressure (PWP) measurements fall between these two numerical predictions. This suggests that at the onset of gas exsolution, the measured pore pressure at the bottom of the sample primarily represents liquid pressure. However, as gas exsolution increases, the measured values more closely reflect a combination of liquid and average fluid pressure. Notably, oscillations in the experimental pore pressure measurements occur within the same pressure range where numerical simulations indicate the onset of divergence between liquid and average pressure trends.
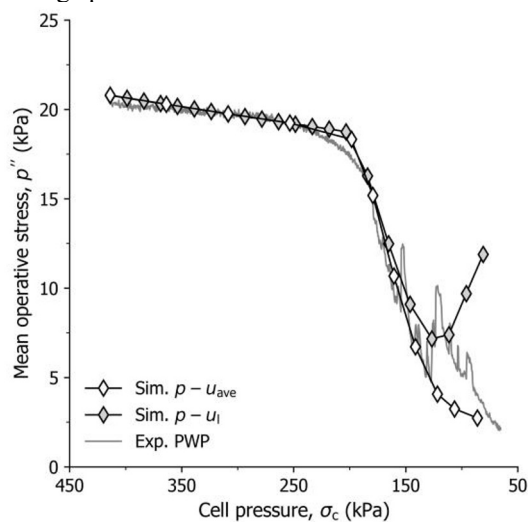

Fig. 8. Evolution of the mean operative stress at the bottom of the sample from Simulation 2 assuming the pore fluid pressure equal to the liquid pressure or average fluid pressure compared with Test 2.

5.2 Gas migration during exsolution

In addition to gas exsolution, gas migration also contributes to the desaturation of the sample. The contours of the degree of saturation at different unloading stages are illustrated in Fig. 9. The lower part of the sample desaturates more quickly than the upper part due to an earlier onset of gas exsolution. Almost half of the sample remains in saturated conditions.

Gas migration facilitates the equilibrium of gas concentrations during the unloading, which can be observed in Fig. 10, where the gas advective flux in the vertical direction from position P1 to P6 is reported. Gas migration is triggered by local gas exsolution, as the nucleated gas creates a pressure difference in the free gas phase. Consequently, gas migration occurs first at P1 at around 200 kPa of cell pressure, but does not occur at P6. The rate of gas flux increases progressively from P1 to P5 as more free gas accumulates and moves toward regions of lower gas pressure.

This advective transport helps the initial gas concentration approach a more uniform distribution during unloading. However, while uniform gassy conditions can gradually develop through gas exsolution,

the volumetric response during unloading must still be interpreted as a boundary value problem.
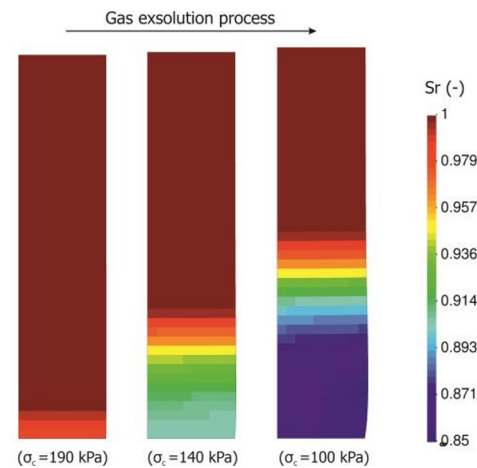

Fig. 9. Contours of saturation degree during gas exsolution process in Simulation 2.
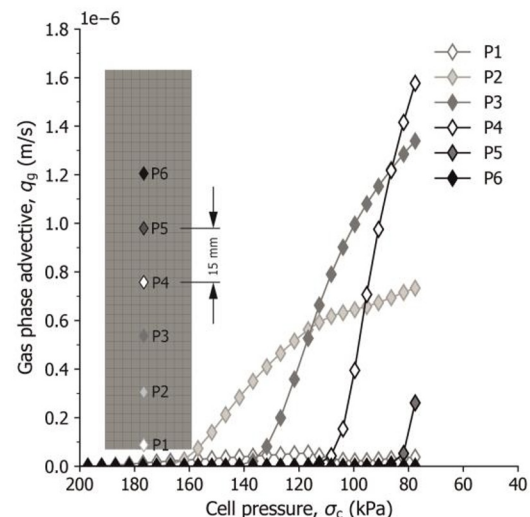

Fig. 10. Advective gas flux in the vertical axis during the undrained unloading from Simulation 2.

5.3 Soil-porous disk interaction

The impact of the porous disk is considered in Simulation 3. As shown in Fig. 11, the mean operative stress, whether calculated using liquid pressure or average fluid pressure at the bottom of the sample, begins to diverge later than in Simulation 2 (Fig. 8). This delay results from interactions between the soil and the porous disk. Fig. 12 shows that the porous disk desaturates quickly due to its low retention capacity, creating local overpressure around it. As a result, liquid pressure at the Bot position rises, delaying gas exsolution. Comparing Fig. 12 with Fig. 9 confirms this effect, as the Bot location in Simulation 3 maintains a higher saturation level than in Simulation 2 before eventually aligning. This overpressure only affects areas near the porous disk, while overall saturation trends remain similar.

The overpressure in the porous disk can be directly assessed through liquid pressure, as depicted by the contours in Fig. 12. A vertical liquid pressure gradient of up to 20 kPa is observed within the porous disk. This

substantial variation of liquid pressure increases the uncertainty in pore pressure measurements beneath the porous disk.
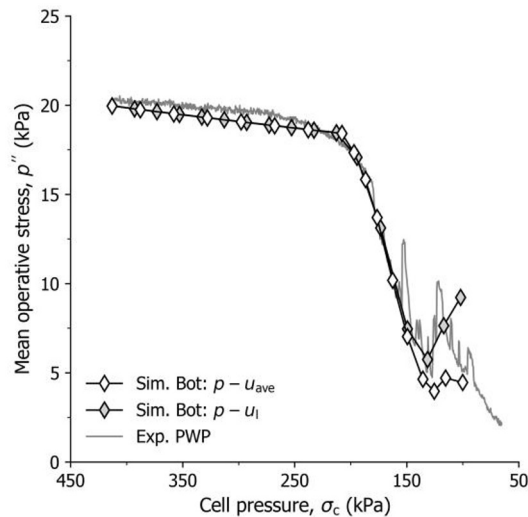

Fig. 11. Evolution of mean operative stress derived from liquid and average fluid pressure at location Bot in Simulation 3.
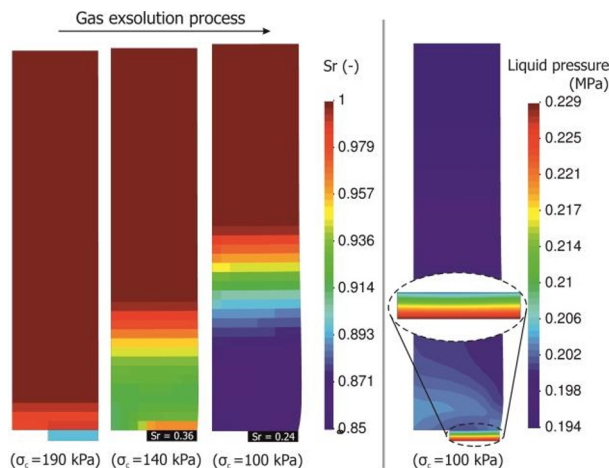

Fig. 12. Contours of saturation degree during gas exsolution process, and of liquid pressure (absolute values) at radial stress of 100 kPa in Simulation 3.

6 Conclusions

This study combines experimental observations with a fully coupled hydro-mechanical finite element model to simulate a triaxial gassy test during gas exsolution. It examines the effects of gas concentration gradients and the porous disk on pore pressure response. The imposed non-uniform gas concentration creates distinct local pore pressure variations, closely matching experimental measurements from local transducers, emphasising the need to analyse gassy tests as boundary value problems.

The global degree of saturation, derived from lateral node displacements, correlates better with the imposed gas pressure gradient than a uniform gas distribution, reflecting spatial variations in gas exsolution. Numerical results indicate that during the last part of the exsolution process, pore pressure measurements from standard transducers beneath the porous disk resemble a combination of local liquid and average fluid pressure

response. Gas migration aligns with the exsolution process and promotes equilibrium in gas concentration due to gas advective flux.

The interaction between the soil and the porous disk mainly affects the adjacent region, leading to localised overpressure and a delay of local exsolution. Additionally, the presence of a substantial vertical liquid pressure gradient within the porous disk complicates the interpretation of pore pressure measurements, adding to the challenges of accurately capturing the pressure response.

References

[1]. J.A. Rosenberry, R.H. Bubier, Water Resour. Res. **39**, 1066 (2003).

[2]. P.H. Glaser, J.P. Chanton, P. Morin, D.O. Rosenberry, D.I. Siegel, O. Ruud, L.I. Chasar, A.S. Reeve, Global Biogeochem. Cycles **18**, GB1003 (2004).

[3]. E.J. Den Haan, G.A.M. Kruse, *Characterisation and Engineering Properties of Natural Soils* **3**, 2101–2133 (2007).

[4]. C. Jommi, S. Muraro, E. Trivellato, C. Zwanenburg, Geotechnique **69**, 753–766 (2019).

[5]. H.F. Zhao, S. Muraro, C. Jommi, Geotechnique Lett. **10**, 461–467 (2020).

[6]. N. Sultan, V. De Gennaro, A. Puech, Geotechnique **62**, 751–766 (2012).

[7]. S. Muraro, C. Jommi, *Modelling free gas overpressure in peat layers*, E3S Web Conf. **195**, 02027 (2020).

[8]. C. Chao, *A comprehensive journey on Dutch organic clays*, Doctoral thesis, Delft University of Technology (2024).

[9]. T. Liu, X. Yang, Y. Zhang, Front. Earth Sci. **10**, 915735 (2022).

[10]. S. Olivella, A. Gens, J. Carrera, E.E. Alonso, Eng. Comput. **13**, 87–112 (1996).

[11]. L.J. Parra-Gómez, S. Muraro, C. Jommi, *An insight into drying-wetting cycles of peat*, E3S Web Conf. **382**, (2023).

[12]. M.T. van Genuchten, Soil Sci. Soc. Am. J. **44**, 892–898 (1980).

[13]. H.F. Zhao, C. Jommi, Can. Geotech. J. **59**, 10, 892–898 (2022).

[14]. E. Trivellato, *The effects of partial saturation on the geotechnical properties of peats: an experimental investigation*, MSc thesis, Politecnico di Milano (2014).

[15]. D.G. Fredlund, Can. Geotech. J. **13**, 386–396 (1976).

[16]. H.S. Yu, Int. J. Numer. Anal. Methods Geomech. **22**, 621–653 (1998).

[17]. C. Jommi, *Experimental evidence and theoretical approaches in unsaturated soils*, 139–153, Balkema Rotterdam (2000).